COMMUNICATIONS

Biomimetics

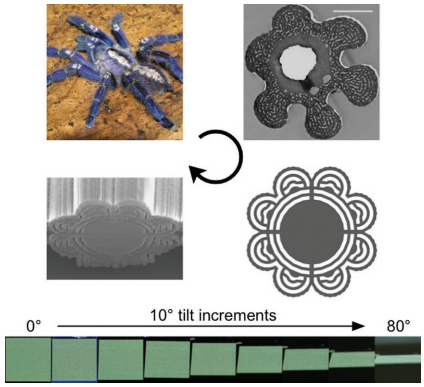

Photonic structures with long-range order are inherently iridescent, suggesting by current theory. Contrary to this paradigm and inspired by biological photonic structures from hairs of blue tarantulas, a noniridescent photonic structure with long-range order is shown here. This photonic structure is hierarchical and has high degrees of rotational symmetry in suitable spatial scales.

ADVANCED OPTICAL MATERIALS
www.advopticalmat.de

Tarantula-Inspired Noniridescent Photonics with Long-Range Order

Bor-Kai Hsiung, Radwanul Hasan Siddique, Lijia Jiang, Ying Liu, Yongfeng Lu, Matthew D. Shawkey, and Todd A. Blackledge*

Pigment-based colorants are used for applications ranging from textiles to packaging to cosmetics.[1] However, structural-based alternatives can be more vibrant, durable, and eco-friendly relative to pigmentary colors.[2] Moreover, optical nanostructures are highly tunable, they can achieve a full color gamut by slight alterations to spacing.[3] However, light interference and/or diffraction from most photonic structures results in iridescence,[4] which limits their broader applications. Iridescent colors that change hue when viewed from different directions are useful for niche markets, such as security and anticounterfeiting,[5] but are not desirable for most applications, such as paints, coatings, electronic displays, and apparels. Hence, fabricating a photonic structure that minimizes iridescence is a key step to unlocking the potential applications of structural colors.

Noniridescent structural colors in nature are produced by coherent scattering of light by quasi-ordered, amorphous photonic structures (i.e., photonic glass),[6–10] or photonic polycrystals[9,11–14] that possess only short-range order. Iridescence is thought to be a fundamental component of photonic structures with long-range order, such as multilayers.[4] However, the complexity of short-range order photonic structures prohibits their design and fabrication using top-down approaches while bottom-up synthesis using colloidal suspension[15,16] or self-assembly[17–20] lack the tight controls over the spatial and temporal scales needed for industrial mass production. Photonic structures with long-range order are easier to model mathematically. Hence, long-range order photonic structures are intrinsically suitable for top-down fabrication, where precise feature placement and scalability can be guaranteed.

Recently, we found blue color produced by multilayer interference on specialized hairs from two species of blue tarantulas (*Poecilotheria metallica* (**Figure 1**a,b) and *Lampropelma violaceopes*) that was largely angle independent.[21] We hypothesize that the iridescent effects of the multilayer are reduced by hierarchical structuring of the hairs. Specifically, the hairs have: (1) high degrees of rotational symmetry, (2) hierarchy—with subcylindrical multilayers surrounding a larger, overarching multilayer cylinder, and (3) nanoscale surface grooves. Because all of these structures co-occur on the tarantulas, it is impossible to decouple them simply by observing nature. Here, we use optical simulation and nano-3D rapid prototyping to demonstrate that introducing design features seen in these tarantulas onto a multilayer photonic structure nearly eliminates iridescence. As far as we are aware, this is the first known example of a noniridescent structural color produced by a photonic structure with both short and long-range order. This opens up an array of new possibilities for photonic structure design and fabrication to produce noniridescent structural colors and is a key first step to achieving economically viable solutions for mass production of noniridescent structural color.

We first design five photonic structures that vary in complexity, incorporating successively more design principles to mimic a real tarantula hair (Figure 1c). The photonic structure designs are illustrated in Figure 1d, and the design principles incorporated in each photonic structure are summarized in **Table 1**. We then simulate each design's optical properties using finite element analyses. Derivative of these designs (i.e., half structures, illustrated in **Figure 2**d,f,h) are also analyzed in the simulation to further decouple the design principles and help to elucidate how their optical properties are affected by each design principle (Table 1).

We then fabricate the photonic designs using nano-3D laser lithography (Figure 1e) to cover an area sufficiently large (Figure 1f) that we can measure their angle-dependency directly with camera and spectrometer under more natural illumination conditions (Figure S1, Supporting Information). The subcylindrical multilayer features in structure #4 approaches the resolution limit of our lithography system. Since the lithography system fabricates in a layer-by-layer manner, it is difficult to fabricate a smooth curved surface when approaching the resolution limits. Therefore, structure #4 is not fabricated because it is beyond the capability of the lithography system (see the Experimental Section for details).

B.-K. Hsiung, Prof. M. D. Shawkey,
Prof. T. A. Blackledge
Department of Biology and Integrated Bioscience Program
The University of Akron
Akron, OH 44325, USA
E-mail: bh63@zips.uakron.edu
Dr. R. H. Siddique[+]
Institute of Microstructure Technology
Karlsruhe Institute of Technology
76344 Eggenstein-Leopoldshafen, Germany
Dr. L. Jiang, Y. Liu, Prof. Y. Lu
Department of Electrical and Computer Engineering
University of Nebraska-Lincoln
Lincoln, NE 68588, USA
Prof. M. D. Shawkey
Biology Department
Terrestrial Ecology Unit
Ghent University
Ledeganckstraat 35, 9000 Ghent, Belgium

[+]Present address: Department of Medical Engineering, California Institute of Technology, Pasadena, CA 91125, USA

DOI: 10.1002/adom.201600599

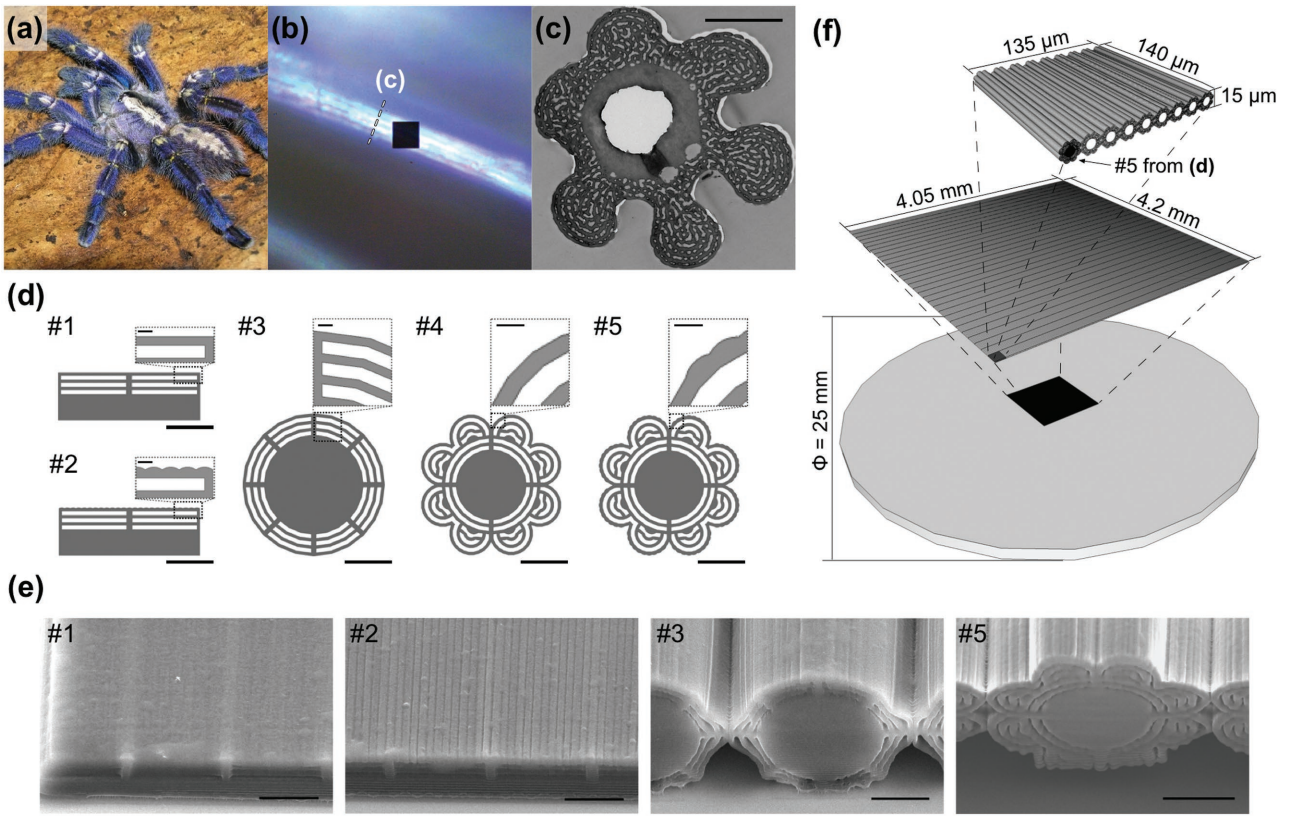

Figure 1. a) An adult female *P. metallica*. Reproduced with permission. Copyright T. Patterson. b) A single blue hair under light microscope. The center black square is 4 μm × 4 μm. c) A transmission electron microscopy image with transverse sectional view of a blue hair. Scale bar = 2 μm. Reproduced with permission. Copyright D. Deheyn, Scripps Institute of Oceanography, University of California, San Diego. d) The transverse sectional view of the photonic designs: structure #1–#5 (Table 1). Scale bar = 5 μm. Inset scale bar = 500 nm. e) The SEM images of structure #1–#5, except #4. Scale bar = 5 μm. f) From top to bottom: (1) a single writing field with nine structures of the same design (here shows structure #5), (2) an assemblage consisting of 900 writing units, and (3) an assemblage on a substrate.

Finite element optical simulation and spectrophotometry of 3D printed prototypes show that high rotational symmetry and hierarchy both individually decrease the angle dependence of multilayer-based photonics (**Figures 2–4**). Rotational symmetry affects angle-dependence more prominently than hierarchy.[22,23] However, neither one eliminates iridescence by itself (Figure 2c,f). Only when both principles are satisfied simultaneously is angle-dependence maximally reduced (Figure 2e). The effects of rotational symmetry and hierarchy seem to be additive, as no conspicuous synergetic effects are observed due to their interaction (Figure 2c–f).

Table 1. Photonic structures and their design principles.

	Design principles			
Photonic structures[a)]	Multilayer	Rotational symmetry	Hierarchy	Surface grooves
#1	X			
#2	X			X
#3	X	X		
#4	X	X	X	
#5	X	X	X	X
#3½	X			
#4½	X		X	
#5½	X		X	X

[a)]½ indicates that it is half of the structure which it follows, as illustrated in Figure 2c, e, g versus Figure 2d, f, h accordingly.

Both simulation and spectrophotometry of 3D printed prototypes show that surface grooves function as a diffraction grating in structure #2 (a striated multilayer), hence further enhancing iridescence (Figures 2b, 3, and 4b). Although simulation shows the tarantula hair-mimic structure with surface grooves (Figure 2g) is more angle dependent than the structure without grooves (Figure 2e), the tarantula hair-mimic structure (structure #5) produces perceptually noniridescent color under diffused omnidirectional illumination (Figures 3 and 4d). This noniridescent color is not produced by pigments because the color disappears under transmission illumination (Figure S2, Supporting Information). Thus, we demonstrate that rotational symmetry and hierarchy together in suitable spatial scales are both necessary and sufficient conditions for ordered, multilayer-based photonics to produce noniridescent structural colors under natural omnidirectional lighting.

The differences between the reflectance spectra predicted by optical simulation and those measured by spectrometry are mainly due to different lighting conditions: while finite element

Adv. Optical Mater. **2016**,
DOI: 10.1002/adom.201600599

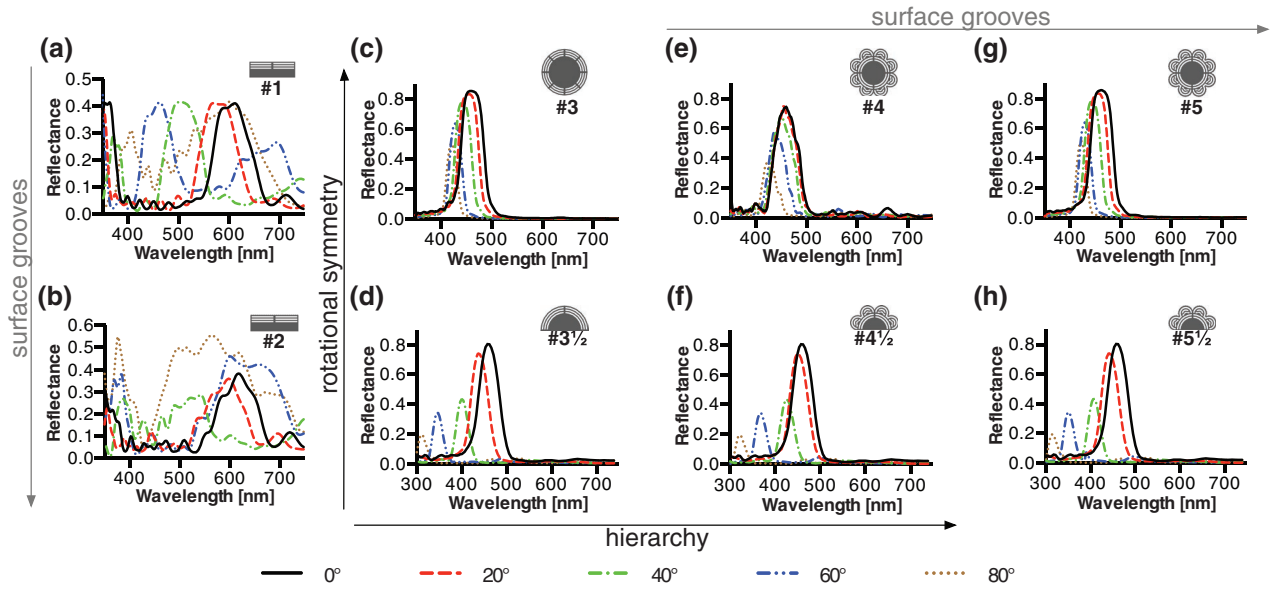

Figure 2. Simulated angle-resolved reflectance spectra for photonic designs. a) Structure #1, simple multilayer. b) Structure #2, multilayer with surface grooves. c) Structure #3, cylindrical multilayer. d) Structure #3½, half cylindrical multilayer. e) Structure #4, hierarchical multilayer cylinder. f) Structure #4½, half hierarchical multilayer cylinder. g) Structure #5, tarantula hair-mimic structure. h) Structure #5½, half-hair mimic. Graphs (c,e,g) add rotational symmetry relative to (d,f,g). Graphs (e,f) add hierarchy compared to (c,d). Graphs (b,g,h) add surface grooves relative to (a,e,f).

simulation considers diffraction and calculates the total reflectance under directional illumination, the spectra measured by the spectrometer are mainly contributed by backscattering under diffused omnidirectional illumination. Also due to the intensive computational demand of finite element simulation, we simplify a 3D problem into 2D simulation, and we neglect the ϕ dependency (varying only θ in one plane) of the structures with planar illumination in the simulation. Structure #1 is flat and does not depend on ϕ incident angle, hence the experimental and simulated results match better. However, other structures might impose ϕ dependency due to their rotational symmetry and hierarchy, which we are unable to calculate in 2D finite element simulation. The limited resolution of nano-3D lithography fabrication process further contributes to this discrepancy. In the original designs (Figure 1d), each layer is 300 nm thick (n = 1.52) and the spacing between the layers is 450 nm with three repeats; while in the fabricated prototypes, both layer thickness and spacing are ≈350 nm. When we change those parameters in structure #1 (a simple multilayer) and perform finite element analyses, the predicted result matches perfectly with the transfer-matrix method-based multilayer interference model[24] (Figure S3, Supporting Information) and closely resembles our measured spectra (Figure 4). This strongly suggests that those peaks, ≈450 and 545 nm in wavelength accordingly, are produced by interference. Under diffused omnidirectional illumination, the peak positions (i.e., hues) are constant (Figure 4a,c,d), hence the hue of the photonic structures is mainly determined by interference (except for structure #2); while the reflectance angle is increased by introducing rotational symmetry and hierarchy into the structural design (Figure 4).

Although the hues are conserved between structure #3 (a simple cylindrical multilayer) and #5 (tarantula hair-mimic structure), structure #3 is conspicuously more iridescent (Figures 3 and 4c,d). This is because the relative reflectance intensity of the two major peaks varies across different angles in structure #3, but remains consistent in structure #5 (Figure S4, Supporting Information). Other than reducing iridescence, surface roughness (through both hierarchy and surface grooves) also increases scattering efficiency, making structure #5 the brightest photonic design in this research (Figure 4d and Figure S5, Supporting Information).

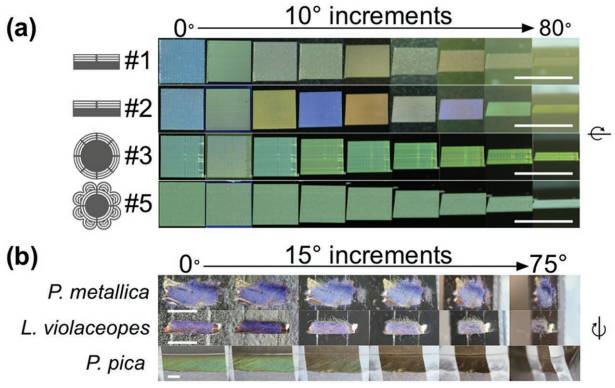

Figure 3. a) Photonic assemblages viewed at varying angles. Structure #1: The color saturation decreased and redshifted with increasing tilting angle due to more random scattering and less interference effects at higher angles (Figure 4a). Structure #2: The color changed even more drastically, oscillating from short to long wavelength colors a couple of times. Structure #3: The color remained largely in green, but the color difference between different angles is still noticeable. Structure #5: No conspicuous color change through the full tilt. b) Comparing the angle dependency with blue tarantula cuticle fragments (*P. metallica* and *L. violaceopes*) and an iridescent bird feather (*P. pica*). Scale bar (white): 5 mm.

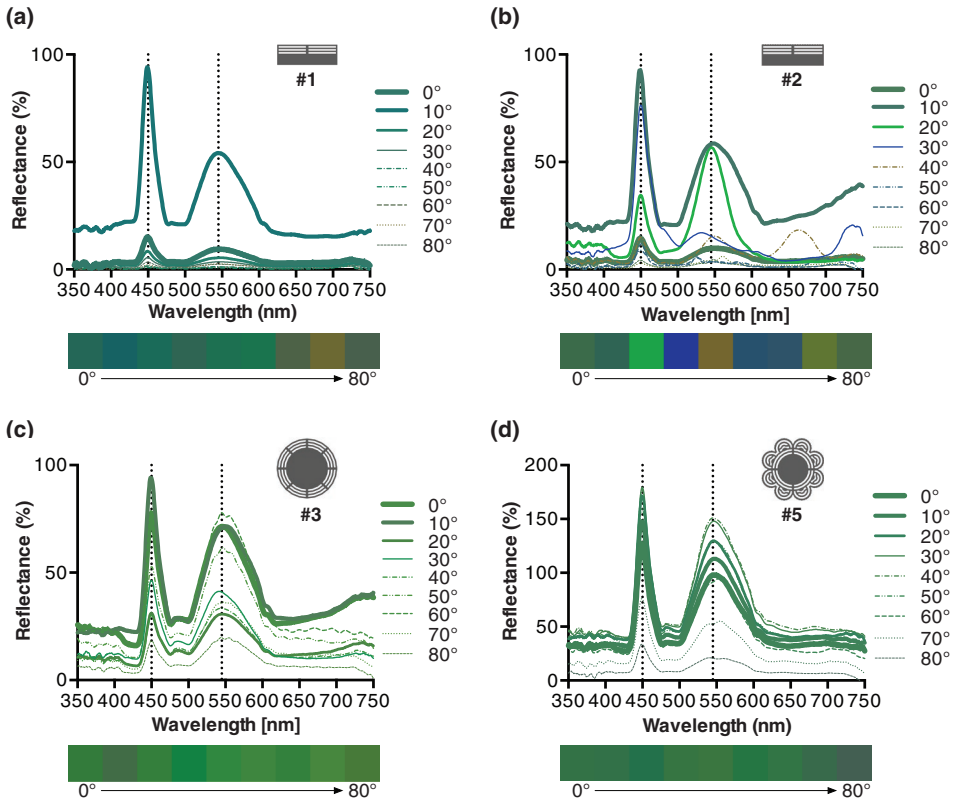

Figure 4. Reflectance spectra of assemblages at different angles. The estimated color tiles below showed good agreement with photos from Figure 3. a) Strong reflectance is limited to a very narrow angle (≈10°). b) High reflectance (>25%) is present up to 40°. However, hue shifted significantly with angle. c) High reflectance is present up to 70°. Both reflectance peaks remain at the same positions, but the relative intensity between two peaks varied (Figure S4, Supporting Information). d) High reflectance is present up to 80°. Both peak positions and peak ratio remains consistent (Figure S4, Supporting Information).

Inspired by the biological photonic structures observed in blue tarantula hairs, we demonstrate that multilayer structures can be modified to produce noniridescent structural colors by introducing micrometer scale rotational symmetry and hierarchy into the photonic design. Moreover, the hues produced by the resulting photonic structures can be predicted readily and accurately by a multilayer interference model using a transfer-matrix method (Figure 4 and Figure S3, Supporting Information). One might argue that the hierarchical feature disrupts the long-range order in our photonic designs, hence producing noniridescent structural colors. If this hypothesis is correct then structure #4½ should also show high angle independence. However, the simulation showed the opposite (Figure 2f) and falsifies this hypothesis. It is also worth noting that the natural models are not completely ordered: the hairs are not perfectly aligned with each other; each hair is not exactly symmetrical; and the layer thickness and spacing are not totally uniform. Our engineered tarantula hair-mimic structures (structure #5) are much more ordered and uniform than the natural models, and consequently they show less iridescence than the natural models (Figure 3). This further agrees with our hypothesis that noniridescent structural color can be produced by highly ordered photonic structures with long-range order, as long as those structures are hierarchical, and with high degrees of rotational symmetry. This approach of producing noniridescent structural colors using photonic structures with long-range order (i.e., modified multilayer) has, to our knowledge, not been explored previously. Our findings reaffirm the value of using nature and the biomimetic process as a tool for innovation and our approach also may help to overcome the current inability of colloidal self-assembly to achieve pure noniridescent structural red due to single-particle scattering and/or multiple scattering.[25] As a result, our research provides a new and easy way for designing structural colorants with customizable hues (see Figure S6, Supporting Information, as one of the potential examples) and iridescent effects to satisfy the needs of different applications. While nano-3D printing of these nanostructures is not viable for mass production, it does identify the key features that are necessary for top-down fabrication. With promising nanofabrication techniques, such as preform drawing[26]—a generally scalable methodology that has been demonstrated for fabricating particles with complex internal architectures and continuously tunable diameters down to nanometer scale[27] – it is possible to mass produce these "designer structural colorants" in an economically viable manner. Our discovery of how to produce noniridescent structural colors using long-range order may therefore lead to a more sustainable future that does not rely upon toxic and wasteful synthetic pigments and dyes.

Adv. Optical Mater. **2016**,
DOI: 10.1002/adom.201600599

Experimental Section

Optical Simulation: 2D optical modeling of the tarantula hair-inspired structures was performed with finite element method (COMSOL Multiphysics) to calculate the angle-resolved reflectance. The exact cross-sectional geometries were considered for simulation which has been used for 3D prototyping. The unit cell was surrounded by 400 nm thick perfectly matched layers (PML) on top and bottom to confine the computational domain. A single bioinspired structure was considered in the unit cell and periodic Floquet boundary conditions were applied in the right and left sides of the cell. The refractive indices of the structures were assumed to be $n = 1.52$ to keep the simulation results in accordance with the experimental ones. Reflectance was calculated for a plane wave by integrating the near-zone scattered field (Poynting vector) over the top boundary before the PML and afterward normalizing with incident intensity. For variable angle of incidences, both the transverse electric (TE) and the transverse magnetic (TM) cases were calculated and averaged (TE + TM/2). The TE wave has the electric field component in the *z* direction, out of the modeling *xy*-plane. For the TM wave, the electric field vector is pointing in the xy-plane and perpendicular to the direction of propagation, whereas the magnetic field has only a component in the *z* direction. All simulation results are plotted in Figure 2.

Nanofabrication: Two-photon polymerization (TPP) fabrication was performed using a 3D laser lithography system (Photonic Professional GT, Nanoscribe GmbH, Germany). A computer-aided design program was used to design and export the surface prototypes as .STL files to a mesh fixing, slicing, and hatching software—DeScribe v2.3.5 (Nanoscribe GmbH). DeScribe translates the files to .GWL files to be then imported to the 3D laser lithography system. The 3D laser lithography system utilized a dip-in configuration with a 63x, 1.4 NA (numerical aperture) oil immersion objective lens (Zeiss, Germany) to focus the laser beam. An acrylic-based monomer liquid photoresist optimized for TPP applications ($n = 1.52$, IP-Dip, Nanoscribe GmbH) was drop casted on a neutral density filter substrate (NE540B-A, Thorlabs, Inc., Newton, NJ, USA) and the objective lens immersed directly in the photoresist. A femtosecond laser (center wavelength of 780 nm, pulse width of 100 fs, repetition rate of 80 MHz, and maximum power of 150 mW) was used as the irradiation source. A laser power of 25 mW was used in the TPP process and was controlled by an acousto-optic modulator. 50 mm s^{-1} writing speed was controlled by a galvo-mirror scanner. After writing, the samples were removed from the sample holder and developed in propylene glycol monomethyl ether acetate (484431, Sigma-Aldrich Co. LLC., St. Louis, MO, USA) for 20 min, followed by a cleaning in isopropyl alcohol before air drying. Nine structures of each design can be written simultaneously within a single writing field (150 µm x 150 µm). A single writing field of each design was first examined using a scanning electron microscopy (SEM) to confirm the prototypes were fabricated according to designs (Figure 1e). Then a total of 900 (30×30) writings were later performed for each photonic design to make an assemblage with sufficient area (Figure 1f) for the subsequent angle-dependence spectrophotometry analyses (Figure S1, Supporting Information).

Scanning Electron Microscopy: The structures were characterized by SEM using a Hitachi S-4700 SEM (Hitachi High-Technologies Corp., Tokyo, Japan). The samples were sputtered-coated with 5 nm of chromium. The imaging voltage was kept low (<10 kV) to avoid damaging the structures.

Spectrophotometry: Assemblages of fabricated photonic structures were mounted on a tilting stage. The tilt angle of the stage was measured by Wixey Digital Angle Gauge (WR300 Type 1, Barry Wixey Development, FL, USA), started in horizontal position (0°) with 10° increments up to 80° (Figure S1, Supporting Information).

Photography: The color of the assemblages at each tilt position was documented by a Canon PowerShot SX60 HS digital camera with Raynox DCR-250 Super Macro Snap-On Lens (Yoshida Industry Co., Ltd., Japan) and Bestlight 48 LED (light-emitting diode) Macro Ring Light. All photos were taken under the same settings at once without postediting, except cropping and resizing (Figure 3).

Spectrometry: The reflectance spectra of the assemblages at each tilt position were measured by AvaSpec-2048 spectrometer with 200 ms integration time, averaging ten scans (Avantes Inc., Broomfield, CO, USA) using Bestlight 48 LED Macro Ring Light as illumination. All measurements were taken relative to Avantes WS-2 reference tile (a white diffuse polytetrafluoroethylene (PTFE)-based material, 100%) and a black velvet cloth (0%). The spectra were then smoothed and plotted using GraphPad Prism statistical software (GraphPad Software, Inc., La Jolla, CA, USA). The colors of spectral curves and tiles in Figure 4 were estimated colors based on smoothed, normalized spectra using "spec2rgb" function in R script "pavo."[28]

Supporting Information

Supporting Information is available from the Wiley Online Library or from the author.

Acknowledgements

The authors thank their backers from Experiment.com (full list in the Supporting Information) and the Sherwin-Williams Company for funding the nano-3D printing. This work was supported by the National Science Foundation (IOS-1257809 to T.A.B.), the U.S. Air Force Office of Scientific Research (FA9550-13-1-0222 to M.D.S.), the Human Frontier Science Program (RGY-0083 to M.D.S.), and the University of Akron Biomimicry Research and Innovation Center. B.-K.H. was supported by the Sherwin-Williams Company under a Biomimicry Fellowship.

Received: July 24, 2016
Revised: September 8, 2016
Published online:

[1] *Pigment Handbook* (Ed: P. A. Lewis), Wiley, Hoboken, NJ, USA **1988**.
[2] A. Saito, *Sci. Technol. Adv. Mater.* **2012**, *12*, 064709.
[3] Y. Yue, T. Kurokawa, M. A. Haque, T. Nakajima, T. Nonoyama, X. Li, I. Kajiwara, J. P. Gong, *Nat. Commun.* **2014**, *5*, 4659.
[4] P. Vukusic, J. R. Sambles, *Nature* **2003**, *424*, 852.
[5] Y. Heo, H. Kang, J.-S. Lee, Y.-K. Oh, S.-H. Kim, *Small* **2016**, *12*, 3189.
[6] R. O. Prum, R. H. Torres, S. Williamson, J. Dyck, *Nature* **1998**, *396*, 28.
[7] R. O. Prum, J. A. Cole, R. H. Torres, *J. Exp. Biol.* **2004**, *207*, 3999.
[8] B. Q. Dong, X. H. Liu, T. R. Zhan, L. P. Jiang, H. W. Yin, F. Liu, J. Zi, *Opt. Express* **2010**, *18*, 14430.
[9] C. Pouya, D. G. Stavenga, P. Vukusic, *Opt. Express* **2011**, *19*, 11355.
[10] B. Q. Dong, T. R. Zhan, X. H. Liu, L. P. Jiang, F. Liu, X. H. Hu, J. Zi, *Phys. Rev. E* **2011**, *84*, 011915.
[11] V. L. Welch, V. Lousse, O. Deparis, A. R. Parker, J. P. Vigneron, *Phys. Rev. E* **2007**, *75*, 041919.
[12] P. Simonis, J. P. Vigneron, *Phys. Rev. E* **2011**, *83*, 011908.
[13] J.-F. Colomer, P. Simonis, A. Bay, P. Cloetens, H. Suhonen, M. Rassart, C. Vandenbem, J. P. Vigneron, *Phys. Rev. E* **2012**, *85*, 011907.
[14] B. D. Wilts, K. Michielsen, J. Kuipers, H. De Raedt, D. G. Stavenga, *Proc. Biol. Sci.* **2012**, *279*, 2524.
[15] Y. Takeoka, M. Honda, T. Seki, M. Ishii, H. Nakamura, *ACS Appl. Mater. Interfaces* **2009**, *1*, 982.
[16] J.-G. Park, S.-H. Kim, S. Magkiriadou, T. M. Choi, Y.-S. Kim, V. N. Manoharan, *Angew. Chem., Int. Ed.* **2014**, *53*, 2899.
[17] M. Harun Ur Rashid, A. Bin Imran, T. Seki, M. Ishii, H. Nakamura, Y. Takeoka, *ChemPhysChem* **2010**, *11*, 579.

[18] J. D. Forster, H. Noh, S. F. Liew, V. Saranathan, C. F. Schreck, L. Yang, J.-G. Park, R. O. Prum, S. G. J. Mochrie, C. S. O'Hern, H. Cao, E. R. Dufresne, *Adv. Mater.* **2010**, *22*, 2939.
[19] Y. Zhang, B. Dong, A. Chen, X. Liu, L. Shi, J. Zi, *Adv. Mater.* **2015**, *27*, 4719.
[20] Y. Ohtsuka, T. Seki, Y. Takeoka, *Angew. Chem.* **2015**, *127*, 15588.
[21] B. K. Hsiung, D. D. Deheyn, M. D. Shawkey, T. A. Blackledge, *Sci. Adv.* **2015**, *1*, e1500709.
[22] J. Dyck, *Biol. Skr. (Copenhagen)* **1987**, *30*, 2.
[23] M. Kolle, A. Lethbridge, M. Kreysing, J. J. Baumberg, J. Aizenberg, P. Vukusic, *Adv. Mater.* **2013**, *25*, 2239.
[24] R. Maia, J. V. O. Caetano, S. N. Báo, R. H. F. Macedo, *J. R. Soc. Interface* **2009**, *6*, S203.
[25] S. Magkiriadou, J.-G. Park, Y.-S. Kim, V. N. Manoharan, *Phys. Rev. E: Stat., Nonlinear, Soft Matter Phys.* **2014**, *90*, 062302.
[26] G. Tao, A. M. Stolyarov, A. F. Abouraddy, *Int. J. Appl. Glass Sci.* **2012**, *3*, 349.
[27] J. J. Kaufman, R. Ottman, G. Tao, S. Shabahang, E.-H. Banaei, X. Liang, S. G. Johnson, Y. Fink, R. Chakrabarti, A. F. Abouraddy, *Proc. Natl. Acad. Sci. USA* **2013**, *110*, 201310214.
[28] R. Maia, C. M. Eliason, P.-P. Bitton, S. M. Doucet, M. D. Shawkey, *Methods Ecol. Evol.* **2013**, *4*, 906.

Adv. Optical Mater. **2016**,
DOI: 10.1002/adom.201600599